BCL2L13 Influences Autophagy and Ceramide Metabolism without Affecting Temozolomide Resistance in Glioblastoma

Courtney Clark[1], Amir Barzegar Behrooz[1], Simone C. da Silva Rosa[1], Joadi Jacobs[1], Xiaohui Weng[2], Abhay Srivastava[3], Rui Vitorino[4], Sudharsan Rao Ande[1], Amir Ravandi[5], Sanjiv Dhingra[3], Stevan Pecic[2], Donald Miller[6], Shahla Shojaei[1¥], Saeid Ghavami[1, 7,8, 9*¥]

[1]Department of Human Anatomy and Cell Science, University of Manitoba College of Medicine, Winnipeg, Canada.

[2]Department of Chemistry & Biochemistry, California State University, Fullerton, 800 N. State College, Fullerton, CA, 92834, United States.

[3]Institute of Cardiovascular Sciences, St-Boniface Hospital Albrechtsen Research Centre, Regenerative Medicine Program, Department of Physiology and Pathophysiology Rady Faculty of Health Sciences, University of Manitoba, Winnipeg, MB, Canada.

[4]Department of Medical Sciences, Institute of Biomedicine-iBiMED, University of Aveiro, Aveiro, Portugal.

[5]Physiology and Pathophysiology, Rady Faculty of Health Sciences, University of Manitoba, Winnipeg, MB, Canada.

[6]Max Rady College of Medicine, Pharmacology and Therapeutics, Room SR438, Kiam Health Sciences Centre, 710 William Avenue, Winnipeg, Manitoba, R3E 3J7, Canada

[7]Faculty of Medicine, Rolna 43, Katowice Poland.

[8]Children Hospital Research Institute of Manitoba, University of Manitoba, Winnipeg, Canada.

[9]Paul Albrechtsen Research Institute, CancerCare Manitoba, University of Manitoba, Winnipeg, Canada.

*Correspondence: Saeid Ghavami, PhD, Associate Professor, Department of Human Anatomy and Cell Science, University of Manitoba College of Medicine, Winnipeg, Canada, Email: Saeid.Ghavami@umanitoba.ca

¥: These authors have co-senior authorship

Abstract

Temozolomide (TMZ) resistance in glioblastoma (GB) poses a significant therapeutic challenge. We developed a TMZ-resistant (TMZ-R) U251 GB model, revealing distinct differences in cell viability, apoptosis, autophagy, and lipid metabolism between TMZ-R and non-resistant (TMZ-NR) cells. TMZ-NR cells exhibited heightened sensitivity to TMZ-induced apoptosis, while TMZ-R cells-maintained viability. Autophagy flux was completely inhibited in TMZ-R cells, indicated by LC3βII and SQSTM1 accumulation. BCL2L13, which showed higher expression in TMZ-R cells, demonstrated increased interaction with Ceramide Synthase 6 (CerS6) and reduced interaction with Ceramide Synthase 2 (CerS2) in TMZ-NR cells. BCL2L13 knockdown (KD) disrupted autophagy flux, decreasing autophagosome accumulation in TMZ-R cells while increasing it in TMZ-NR cells. These changes contributed to altered ceramide profiles, where TMZ-R cells displayed elevated levels of Cer 16:0, 18:0, 20:0, 22:0, 24:0, and 24:1. Our findings highlight BCL2L13 and altered ceramide metabolism as potential therapeutic targets to overcome TMZ resistance in GB.

Keywords: BCL2L13, Autophagy Flux, CerS-BCL2L13 Interaction, Temozolomide-Resistant Glioblastoma Cells

INTRODUCTION

Glioblastoma (GB) is the most aggressive and lethal primary brain tumor, with a median survival of only 15 months despite aggressive multimodal treatment [1, 2]. One of the significant challenges in treating GB is the development of resistance to temozolomide (TMZ), the standard chemotherapy for this disease [3]. The underlying mechanisms driving TMZ resistance (TMZ-R) involve complex cellular processes, including alterations in autophagy, apoptosis, and lipid metabolism [4, 5]. Understanding these processes is crucial for developing strategies to overcome resistance and improve therapeutic outcomes.

Autophagy is a critical cellular process that involves the degradation and recycling of cellular components to maintain homeostasis. Autophagy plays a dual role in cancer, acting as a tumor suppressor and a survival mechanism [6, 7]. In TMZ-R GB cells, our recent findings have shown that autophagy flux is inhibited, as evidenced by the accumulation of autophagy markers such as LC3βII and SQSTM1 [8]. This inhibition suggests a blockage in the autophagic process, potentially allowing these cells to evade apoptosis—a process typically activated in response to cellular stress and damage induced by chemotherapy [8]. These results indicate that the disruption of autophagy flux in TMZ-R cells is a critical factor in developing resistance, as it may enable the cells to withstand the cytotoxic effects of TMZ.

BCL2L13, a member of the BCL-2 family of proteins, has been identified as a crucial regulator of apoptosis and ceramide synthesis in cancer cells [9-11]. In GB, BCL2L13 is highly expressed and plays a significant role in regulating the synthesis of ceramides, a class of lipids involved in promoting apoptosis [10]. Our study further reveals that BCL2L13 interacts with ceramide synthases CerS2 and CerS6, inhibiting their activity and thus affecting the balance of ceramides within the cell. This modulation of ceramide levels by BCL2L13 potentially contributes to the survival of GB cells under TMZ treatment, as ceramides are known to induce apoptotic pathways that can lead to cell death [12, 13]. Given the role of BCL2L13 in regulating autophagy flux and ceramide synthesis [8, 10], we hypothesize that BCL2L13 contributes to TMZ resistance in GB by modulating these pathways. Specifically, we propose that the elevated expression of BCL2L13 in TMZ-R GB cells disrupts autophagy flux and alters ceramide metabolism, leading to enhanced survival of resistant cells. This study aims to elucidate the mechanistic roles of BCL2L13 in TMZ-R GB cells, focusing on its interactions with autophagy, ceramide pathways, and ceramide synthases and exploring the potential of targeting BCL2L13 as a therapeutic strategy to overcome TMZ resistance.

To test this hypothesis, we conducted a detailed analysis of autophagy flux, apoptosis, and ceramide profiles in TMZ-R and TMZ-NR GB cells with varying levels of BCL2L13 expression. Our objectives were to determine how BCL2L13 influences autophagy, ceramide synthesis, and apoptosis in the context of TMZ resistance and to assess whether targeting BCL2L13 could restore sensitivity to TMZ and improve therapeutic outcomes in GB. The findings from this study provide new insights into the molecular mechanisms underlying TMZ resistance and suggest novel therapeutic targets to enhance the effectiveness of GB treatment.

MATERIALS AND METHODS

Cell Culture

All experiments used the U251 human glioblastoma cell line. Cancer cells were cultured in Dulbecco's Modified Eagle's Medium-high glucose (4 mg/ml) (DMEM) (CORNING; Cat #: 50-003-PB) supplemented with 10% Fetal Bovine Serum (FBS) (Gibco™; Cat #: 16000044) and 1% penicillin and streptomycin. Cells were maintained in a humidified incubator in standard cell culture conditions (95% air and 5% CO_2 at 37°C). Stable BCL2L13 knockdown (KD) and negative control (scramble) were grown in the same medium plus puromycin (4 μg/ml) to ensure the selection of stably transfected cells.

Preparation of TMZ-Resistant Cells

U251-mKate cells (developed by Dr. Marcel Bally, Experimental Therapeutics, British Columbia Cancer Agency, Vancouver, BC, Canada) were cultured in T75 tissue culture flasks in a complete media containing high glucose DMEM, 10% FBS (Gibco; Cat #:10437-036), and 1% Penicillin-Streptomycin (Gibco, Cat #:15140122) and incubated at 37°C, 5% CO_2, in a humidified incubator (Thermo Fischer Scientific, US). A pulsed-selection strategy was chosen to make a clinically relevant chemoresistant model [14]. Once cells reached 70% confluence, they were treated with 100μM TMZ (Sigma Aldrich, CAS #: 85622-93-1) over three weeks, followed by four weeks of TMZ-free media for recovery. Cells were cultured in complete media with 250μM TMZ for three weeks, followed by another four weeks with TMZ-free media. The final population of U251-mKate cells resistant to 250μM TMZ was selected and cultured in a complete media without TMZ for four weeks.

Immunoblotting

Protein expression was detected using western blotting, with GAPDH and Ponceau S as loading controls. Cells were lysed in buffer (20 mM Tris-HCl pH 7.5, 0.5 mM PMSF, 0.5% Nonidet P-40, 100 μM β-glycerol 3-phosphate, 0.5% protease and phosphatase inhibitor cocktail), and lysates were centrifuged at 10,000 g for 10 min at 4°C. Protein concentration was determined by Lowry assay. Proteins were separated by SDS-PAGE and transferred to PVDF membranes. After blocking with 5% skim milk in TBST for 1 hour at room temperature, membranes were incubated overnight at 4°C with primary antibodies in 1% skim milk/TBST, followed by HRP-conjugated secondary antibodies for 2 hrs at room temperature. Detection was performed using ECL (Amersham-Pharmacia Biotech) and visualized with a BioRad imager. Band intensity was quantified using Alpha Ease FC software [15, 16].

Transmission Electron Microscopy (TEM)

Autophagy was confirmed using TEM. Briefly, U251 GB cells were cultured in 100mm dishes in DMEM (10% FBS 1% P/S) in standard cell culture incubator conditions. Cells were fixed in Karnovsky fixative for 1 hour at 4°C, and the pellet was resuspended in 5% sucrose in 0.1M Sorenson's phosphate buffer overnight at 4°C. Cells were pelleted and post-fixed with 1% osmium tetroxide in 0.1M Sorenson's buffer for 2 hours. Next, cells were dehydrated and embedded in Embed 812 resin for sectioning. Thin sections (200 nm) were cut and placed on copper grids for staining and counter-staining with uranyl acetate and lead nitrate, respectively. Imaging was done using a Philips CM10 electron microscope [17, 18].

Immunocytochemistry (ICC)

Changes in autophagy in U251 GB cells and BCL2L13 knockdown transfectants were detected using immunocytochemistry. Cells were fixed with 3.7% formaldehyde for 30 mins at room temperature, washed thrice with DPBS, and permeabilized overnight at 4°C in blocking buffer (5% IgG-free BSA, 0.3% Triton X-100 in DPBS). The blocking buffer was then replaced with antibody solution (1% BSA, 0.3% Triton X-100, and conjugated antibodies in DPBS), and samples were incubated overnight at 4°C in the dark. Anti-LC3 primary antibody (1:2000, Sigma) and donkey anti-rabbit IgG secondary antibody (1:2000, Jackson ImmunoResearch) were used. After staining, samples were washed, incubated with DPBS, and stored at 4°C in the dark until imaging. Imaging was performed using a Zeiss Axiovert 200 microscope with Calibri 7 LED Light Source and Axiocam 702 mono camera. Image processing and quantification were done using Fiji (ImageJ) and Zen 2.3 Pro software. All experiments were independently repeated 3 times, with a minimum of 10 images captured per condition [19, 20].

MTT Viability Assay

Cell viability of U251 GB cells (TMZ-NR, TMZ-R, BCL2L13 KD, and WT) was measured using the MTT assay. Cells were cultured to 50% confluence in high glucose DMEM with 10% FBS and 1% P/S, then seeded (TMZ-NR: 50,000 cells/mL; TMZ-R: 75,000 cells/mL) in 96-well plates. Cells were treated with varying concentrations of BafA1 (1, 5, or 10nM) for 72h. MTT (20µL of 5mg/mL) was added to each well, and plates were incubated at 37°C with 5% CO2 for 3 hrs. The media was aspirated, and 200µL of DMSO was added to dissolve the formazan crystals. After 25 mins incubation at RT in the dark, absorbance was measured at 570nm using a Synergy H1 Microplate Reader. Relative cell viability was calculated as the percentage of control using the formula: (mean OD570 of treated cells/mean OD570 of control cells) x 100 [21, 22].

Production of Stable BCL2L13 Knock Down (KD) Cell Line

U251 TMZ-R and NR GB cells were seeded in 12-well plates and cultured in DMEM (10% FBS, 1% P/S). At 40% confluency, cells were treated with 10 µg/mL polybrene in DMEM (without FBS) for 1 hour, followed by infection with lentiviruses carrying shRNA targeting BCL2L13 or scramble RNA (scRNA) as a control. After 12 hours of incubation, media were refreshed, and cells were allowed to recover for 48 hours. The transfection process was repeated to enhance efficiency. Transfected cells were selected with 4 µg/mL puromycin. Successful knockdown of BCL2L13 was confirmed by western blotting in stable clones [23].

Flow Cytometry/Cell Cycle Analysis

U251 GB cells (TMZ-NR, TMZ-R, BCL2L13-WT, BCL2L13-KD) were seeded in 12-well plates (50,000 cells/well for TMZ-sensitive and 75,000 cells/well for TMZ-resistant cells) and grown to 60% confluence. Cells were treated with 250 µM TMZ for 48 or 96 hours. Post-treatment, cells were detached with EDTA buffer, harvested by centrifugation, and washed in PBS. They were resuspended in hypotonic PI lysis buffer (0.01% Triton X-100, 1% sodium citrate, 40 µg/mL propidium iodide) and incubated at room temperature in the dark for 30 minutes. Flow cytometry was performed using a Beckman Coulter Cytoflex LX with a 488 nm laser and 610/20 BandPass filter to measure the percentage of cells in Sub-G0, G0-G1, S, and G2-M phases [24, 25].

Measurement of Mitochondrial Respiration: Sea Horse Assay

Oxygen consumption rate (OCR) was assessed using the Agilent Seahorse XFe24 analyzer. U251 cells (TMZ-NR, TMZ-R, BCL2L13-KD, and scramble) were seeded in XF 24-well microplates at 0.3 x 10□ cells/well. On the experiment day, cells were switched to XF base minimal DMEM with glucose, L-glutamine, and sodium pyruvate, then incubated at 37°C for 1 hour. Baseline OCR was measured, followed by protein leak (1 µM oligomycin), maximal respiration (2 µM FCCP), and non-mitochondrial respiration (1 µM rotenone, 1 µM antimycin A). OCR normalization was performed using live cell counts stained with Hoechst33342. Maximal respiration was calculated as FCCP OCR minus non-mitochondrial OCR; spare capacity as FCCP OCR minus baseline OCR; ATP production as baseline OCR minus Oligomycin OCR; and proton leak as Oligomycin OCR minus non-mitochondrial OCR. Data are presented as pmol O□/min/cell count.

Co-Immunoprecipitation (Co-IP) for BCL2L13 Interaction with CerS2 and CerS6 in U251 TMZ-R and TMZ-NR Cells

U251 TMZ-resistant (TMZ-R) and non-resistant (TMZ-NR) glioblastoma cells were lysed in buffer (20 mM Tris-HCl, pH 7.5, 150 mM NaCl, 1% NP-40, 0.5% sodium deoxycholate, 1 mM EDTA, 1 mM PMSF, 10% glycerol, protease/phosphatase inhibitors). Lysates were pre-cleared with Protein A/G agarose beads, then incubated overnight at 4°C with anti-BCL2L13 antibody, followed by a 2-hour incubation with fresh beads. Immunocomplexes were washed, eluted in 2X SDS-PAGE sample buffer, and analyzed via Western blot using antibodies against CerS2 and CerS6. Densitometry was performed to quantify interactions.

Phase Contrast

Bright-field images were taken using an Axio Observer ZEISS microscope (ZEISS, Oberkochen, Germany) using 20x and 50x magnification objectives. Quantification, scale bars, background subtraction, and processing were done on Fiji (ImageJ) and Zen 2.3 Pro software.

Liquid Chromatography-Mass Spectrometry (LC-MS) for Lipidomics Analysis of Ceramide Species

Lipids were extracted from U251 GB cells (NR, R, BCL2L13-KD, BCL2L13-WT) using a chloroform

(2:1, v/v) mixture. Cells grown to confluence were collected, sonicated, and centrifuged (1000g, 10 min). The supernatant was mixed with the internal standard (ISTD), vortexed, and centrifuged (3500 rpm, 5 min). The lower phase was dried under N□ gas and reconstituted in water-saturated butanol, followed by methanol with 10 mM ammonium formate. After centrifugation (10000g, 10 min), lipids were analyzed by LC-MS. Separation was performed on a Zorbax C18 column using a linear gradient of mobile phases A and B, both containing 10 mM ammonium formate. The elution program involved increasing from 0% to 100% mobile phase B over 8 minutes, with re-equilibration to starting conditions before the next injection. Diacylglycerol and triacylglycerol species were separated isocratically at 100 µl/min. The column was maintained at 50°C, and the injection volume was 5 µl.

Mass Spectral Analysis

Lipidomic analysis was competed as previously described [26]. Briefly, lipids eluted from the HPLC system were introduced into the AbSciex 4000 QTRAP triple quadrupole linear hybrid mass spectrometer. The mass spectrometer was operated in scheduled Multiple Reaction Monitoring (MRM) mode. 322 unique lipids spanning 25 lipid classes/subclasses were screened for targeted semi-quantitation. All lipid species other than fatty acids were scanned in positive electrospray ionization mode [ESI+]. The individual lipids in each lipid class were identified by lipid class-specific precursor ions or neutral losses. Lipids were then quantified by comparing the deisotoped lipid peak areas against those of the class-specific ISTDs added before lipid extraction. The total carbon number of the fatty acids represented lipids. In ESI+ mode, the instrument settings were optimized as follows: curtain gas (psi), 26; collision gas (nitrogen), medium; ion spray voltage (V), 5500; temperature (°C), 500.0; ion source gas 1 (psi), 40.0; ion and source gas 2 (psi), 30.0. The MRM detection window was fixed between 45s and 90s depending upon the chromatographic peak width of the lipid class. Isobaric species within the same class, such as PC(O) and PC(P), exhibited clear separation in this method. Also, molecular species within the same lipid class, which differ only in the number of double bonds, were well separated chromatographically. All analyses were performed with R software (version 4.1.1). Limma, pheatmap, and ggplot2 packages were used.

Statistics and reproducibility

All experiments were conducted in triplicate, with three independent repeats. Data are presented as mean ± standard deviation. Statistical significance was determined using a two-tailed t-test or one-way/two-way ANOVA with Tukey's post hoc test for multiple comparisons, considering p-values ≤ 0.05 as significant. Lipid classification and annotation were performed using the LIPIDMAPS database. Lipidomic data were analyzed with MetaboAnalyst 5.0, including hierarchical clustering, principal component analysis (PCA), and partial least squares discriminant analysis (PLSDA) to identify differential lipids.

RESULTS

Temozolomide induces more cell death in U251 Temozolomide non-resistant GB cells.

We found that U251 TMZ-resistant (TMZ-R) glioblastoma (GB) cells maintained 50% viability at TMZ concentrations up to 500μM ($P < 0.0001$), compared to significant cell death in TMZ-non-resistant (TMZ-NR) cells (Fig. 1A). TMZ-R cells were maintained in 250μM TMZ, with the drug removed 24 hours before treatment. Phase contrast microscopy revealed that TMZ-NR cells showed reduced confluence and increased cell death after 48 hours of treatment with 100μM TMZ, while TMZ-R cells remained unaffected (Fig. 2B). TMZ-NR cells were smaller, rounder, and had shorter filopodia; in contrast to the elongated filopodia of TMZ-R cells. Nicolletti apoptosis assay confirmed that TMZ significantly increased the sub-G0 apoptotic phase ($P < 0.0001$) and altered cell cycle distribution in TMZ-NR cells, with no significant effects on TMZ-R cells (Fig. 1C-E). No significant changes were observed in the S phase for either cell type following treatment ($P > 0.05$) (Fig. 1F).

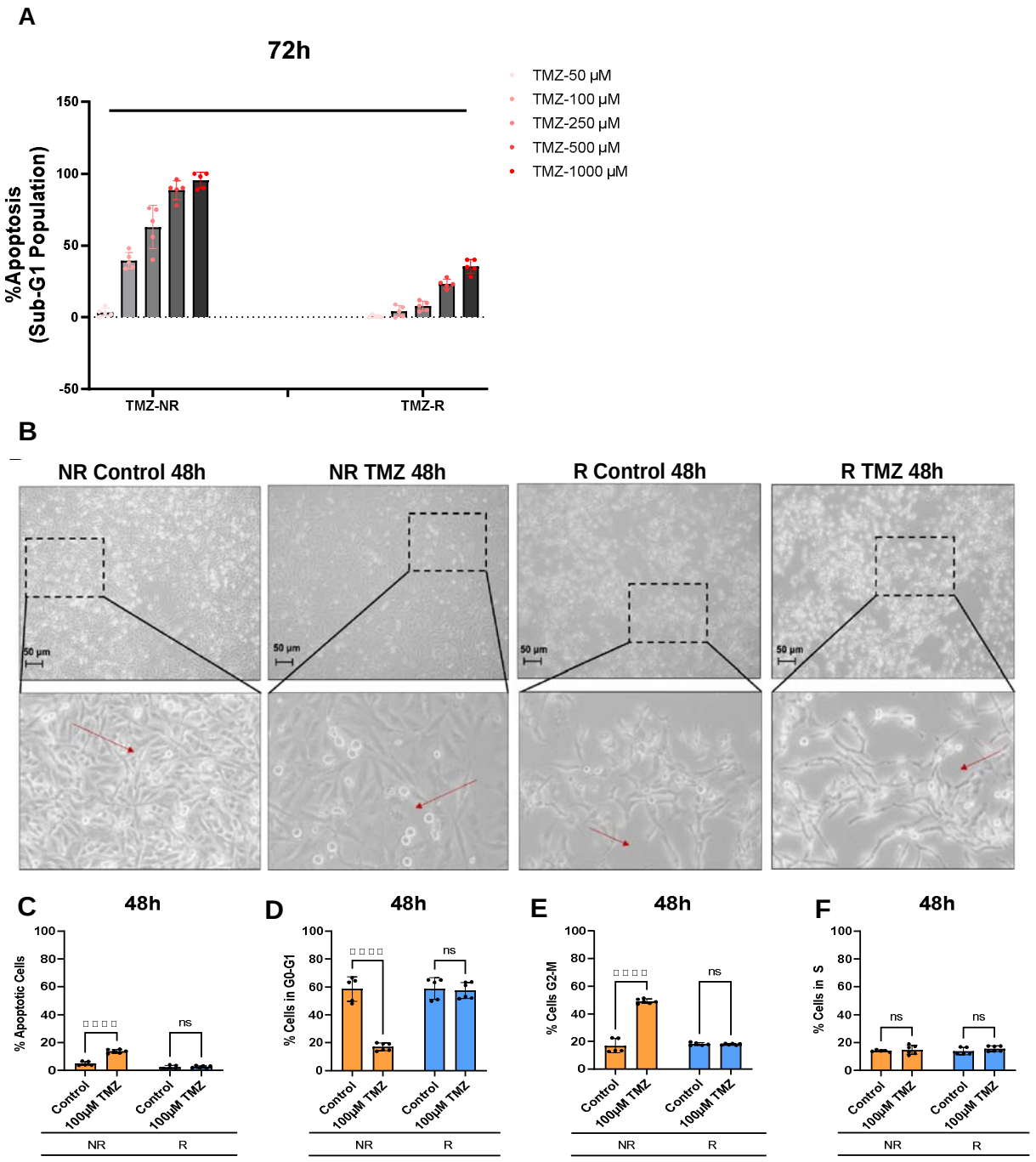

Figure 1 Temozolomide induces more cell death in U251 Temozolomide NR cells. A U251 TMZ-resistant (R) and non-resistant (NR) cells were treated with 10–5000 µM TMZ, and apoptosis was assessed over 72 hours using the Nicolleti assay. **B** Phase-contrast images of TMZ-R and TMZ-NR cells after 48-hour treatment with 100 µM TMZ show more apoptotic morphology in TMZ-NR cells. **C-F** TMZ (100 µM) treatment induced significantly higher apoptosis and

increased G2/M phase arrest in TMZ-NR cells compared to TMZ-R cells, which showed no significant change. Data represent mean ± SD of three independent experiments.

Autophagy flux is inhibited in TMZ-Chemoresistant GB cells.

We investigated autophagic activity in U251 TMZ-resistant (TMZ-R) and non-resistant (TMZ-NR) glioblastoma (GB) cells by assessing LC3βII and SQSTM1 (p62) expression levels using immunoblotting. LC3βII and SQSTM1, key autophagy markers, were degraded over 72 hours in TMZ-NR cells, indicating active autophagy. In contrast, their accumulation in TMZ-R cells suggested a significant disruption in autophagy flux ($P < 0.01$) (Fig. 2A, B). To further examine autophagy, we used Bafilomycin A1 (BafA1), an inhibitor of vacuolar H (+)-ATPase that blocks autophagy flux. MTT assays demonstrated that BafA1 (10 nM) significantly reduced the viability of TMZ-NR cells ($P < 0.001$) but had no cytotoxic effect on TMZ-R cells (Fig. 2C). Subsequently, we selected 5 nM BafA1 to compare autophagy flux between TMZ-R and TMZ-NR cells. In TMZ-NR cells, BafA1 treatment increased LC3βII and SQSTM1 levels ($P < 0.01$), whereas in TMZ-R cells, BafA1 had no significant impact, suggesting complete disruption of autophagy at the autophagosome-lysosome fusion stage (Fig. 2D, E). Immunocytochemistry (ICC) confirmed these findings, showing more LC3β puncta in TMZ-R cells, indicative of accumulated autophagosomes (Fig. 2F). Additionally, transmission electron microscopy (TEM) revealed a significantly higher number of double-membrane vacuoles in TMZ-R cells compared to TMZ-NR cells, further supporting the conclusion that autophagy is disrupted in TMZ-R cells (Fig. 2G, H).

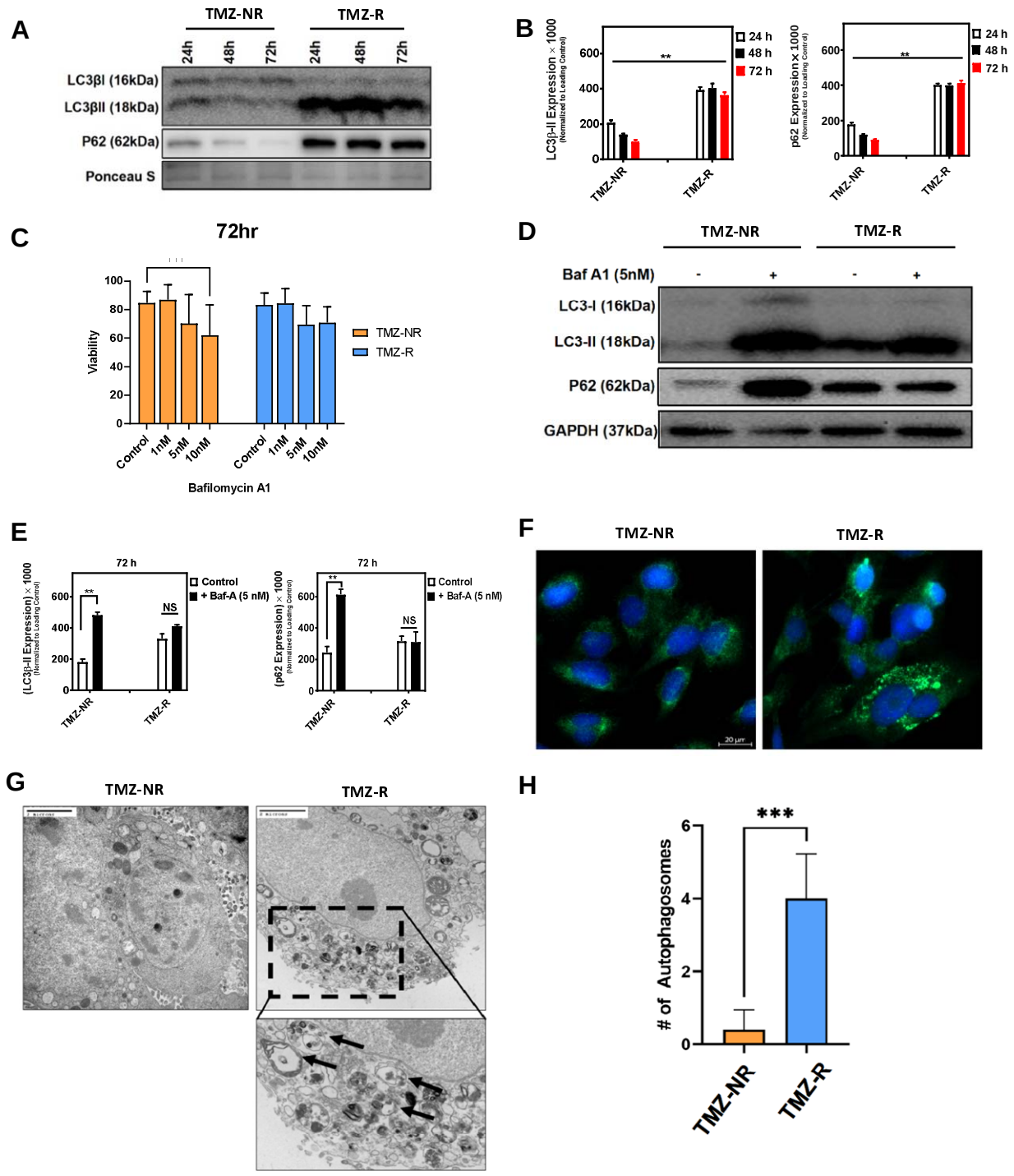

Figure 2 Autophagy flux is inhibited in TMZ-R cells. A, B U251 TMZ-NR and TMZ-R cells were cultured for 72 hours with lysates collected every 24 hours for immunoblotting. Autophagy markers (p62 degradation, LC3β lipidation, and LC3βII formation) were assessed, showing active autophagy flux in TMZ-NR cells over time, but inhibition in TMZ-R cells ($P < 0.01$). Data represent three biological replicates. **C** Cytotoxic effects of Bafilomycin-A1 (1, 5, 10nM) on TMZ-NR and TMZ-R cells over 72 hours were measured by MTT assay, revealing significant cell death induction in TMZ-NR cells at 10nM

(P < 0.001), with minimal effect on TMZ-R cells. **D, E** Immunoblot analysis of TMZ-NR and TMZ-R cells treated with 5nM Bafilomycin-A1 for 72 hours, with lysates collected every 24 hours, demonstrated inhibited autophagy flux in TMZ-NR cells (P < 0.01) but no effect in TMZ-R cells. GAPDH was the loading control. **F** Immunocytochemistry for LC3β puncta showed increased autophagosome formation in TMZ-R cells relative to TMZ-NR cells. **G, H** TEM images (25,000x) of TMZ-NR and TMZ-R cells demonstrated significantly more double-membrane autophagic vacuoles in TMZ-R cells (P < 0.001), with quantification across 10 cells.

BCL2L13 has higher expression in U251 TMZ-R compared to TMZ-NR GB cells.

BCL2L13 expression was examined in U251 TMZ-resistant (TMZ-R) and non-resistant (TMZ-NR) glioblastoma (GB) cells using immunoblotting, with samples collected every 24 hours over 72 hours. The results demonstrated significantly higher BCL2L13 expression in TMZ-R cells compared to TMZ-NR cells at the 48 and 72-hour time points ($P < 0.01$) (Fig. 3A, B). Given the known roles of BCL2L13 in apoptosis regulation and mitochondrial function, we further explored its impact on autophagy and cell survival in TMZ-R cells. To investigate the effects of BCL2L13 on autophagy, apoptosis, and TMZ response, BCL2L13 was knocked down in U251 TMZ-R and TMZ-NR cells via lentiviral transfection, achieving stable RNA silencing (Fig. 4C). Transmission electron microscopy (TEM) revealed that BCL2L13 knockdown (KD) did not significantly alter the number of cytosolic double-membrane vacuoles in either TMZ-NR or TMZ-R cells ($P > 0.05$) (Fig. 3C, D). Autophagy flux was further assessed using Bafilomycin A1 (Baf-A1, 5 nM, 72 hours). In TMZ-NR cells, BCL2L13 KD significantly increased LC3β-II levels, while in TMZ-R cells, it significantly decreased LC3β-II without Baf-A1 treatment (Fig. 3E, F). Additionally, BCL2L13 KD did not significantly affect SQSTM1 degradation in TMZ-NR cells but significantly reduced SQSTM1 degradation in TMZ-R cells (Fig. 3E, F). Baf-A1 treatment significantly increased LC3β-II and decreased SQSTM1 degradation in TMZ-NR cells, irrespective of BCL2L13 expression, while not affecting these markers in TMZ-R cells (Fig. 3G, H). These findings suggest that BCL2L13 is key in regulating autophagy flux, particularly in TMZ-R cells where autophagy is inhibited. Finally, we evaluated the impact of BCL2L13 expression on TMZ-induced apoptosis and cell cycle distribution using flow cytometry. BCL2L13 expression did not significantly alter apoptosis in either TMZ-NR or TMZ-R cells after 48 and 96 hours of TMZ treatment ($P > 0.05$). However, BCL2L13 KD in TMZ-NR cells led to a significant reduction in the percentage of cells in the G2-M phase after 48 hours, while TMZ-R cells (both scramble and BCL2L13 KD) showed a decrease in the G0-G1 phase after 96 hours of treatment (Fig. 3H, I).

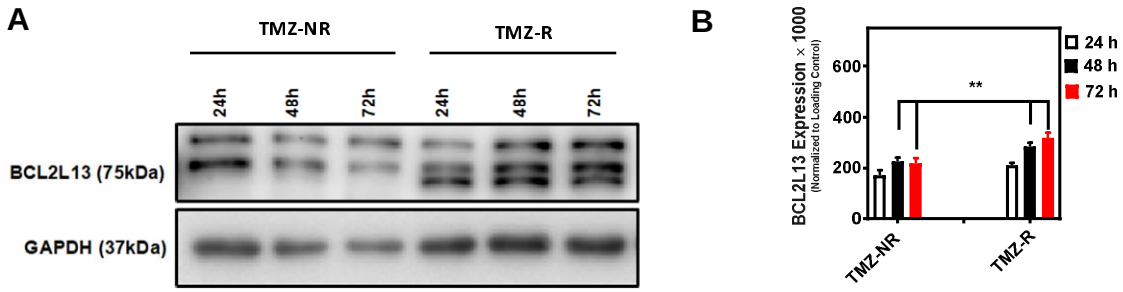

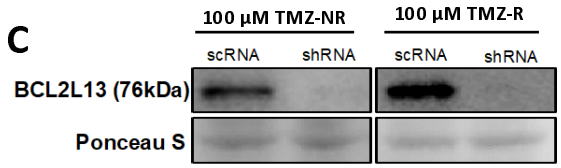
C
100 µM TMZ-NR
100 µM TMZ-R
scRNA
shRNA
scRNA
shRNA
BCL2L13 (76kDa)
Ponceau S

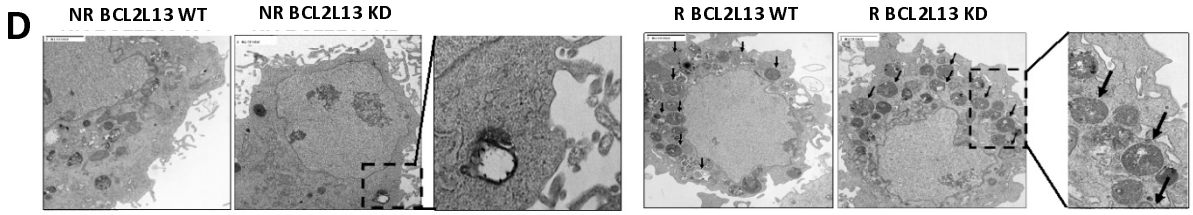
D
NR BCL2L13 WT
NR BCL2L13 KD
R BCL2L13 WT
R BCL2L13 KD

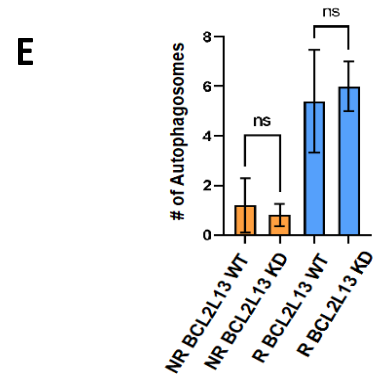
E
# of Autophagosomes
ns
ns
NR BCL2L13 WT
NR BCL2L13 KD
R BCL2L13 WT
R BCL2L13 KD

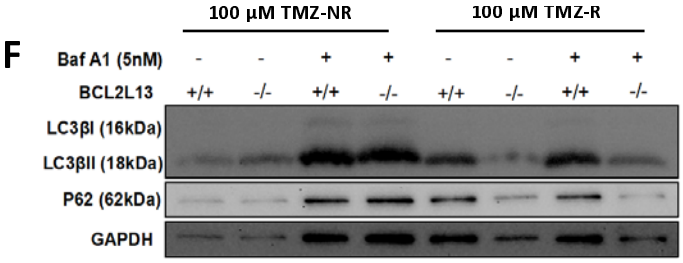
F
100 µM TMZ-NR
100 µM TMZ-R
Baf A1 (5nM)
BCL2L13
LC3βI (16kDa)
LC3βII (18kDa)
P62 (62kDa)
GAPDH

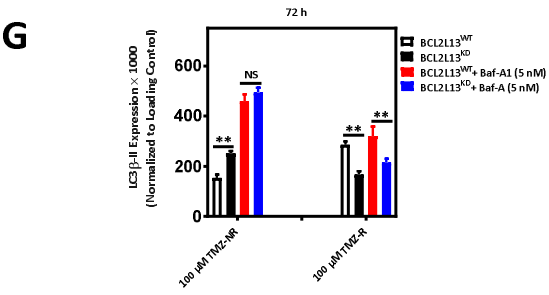
G
72 h
LC3β-II Expression × 1000 (Normalized to Loading Control)
BCL2L13WT
BCL2L13KD
BCL2L13WT+ Baf-A1 (5 nM)
BCL2L13KD+ Baf-A (5 nM)
100 µM TMZ-NR
100 µM TMZ-R

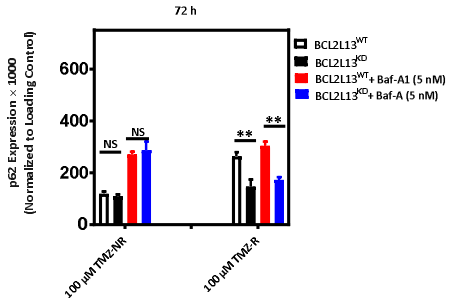
72 h
p62 Expression × 1000 (Normalized to Loading Control)
BCL2L13WT
BCL2L13KD
BCL2L13WT+ Baf-A1 (5 nM)
BCL2L13KD+ Baf-A (5 nM)
100 µM TMZ-NR
100 µM TMZ-R

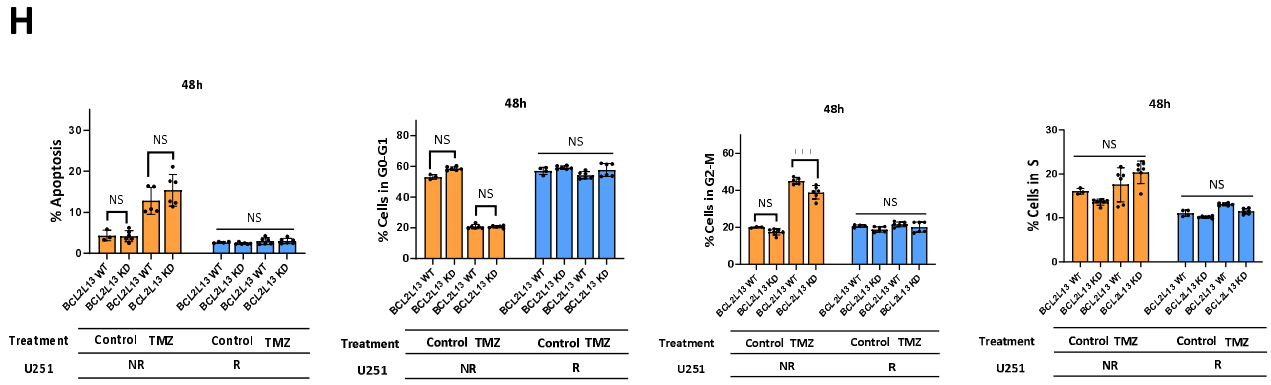
H
48h
% Apoptosis
% Cells in G0-G1
% Cells in G2-M
% Cells in S
Treatment
Control
TMZ
U251
NR
R

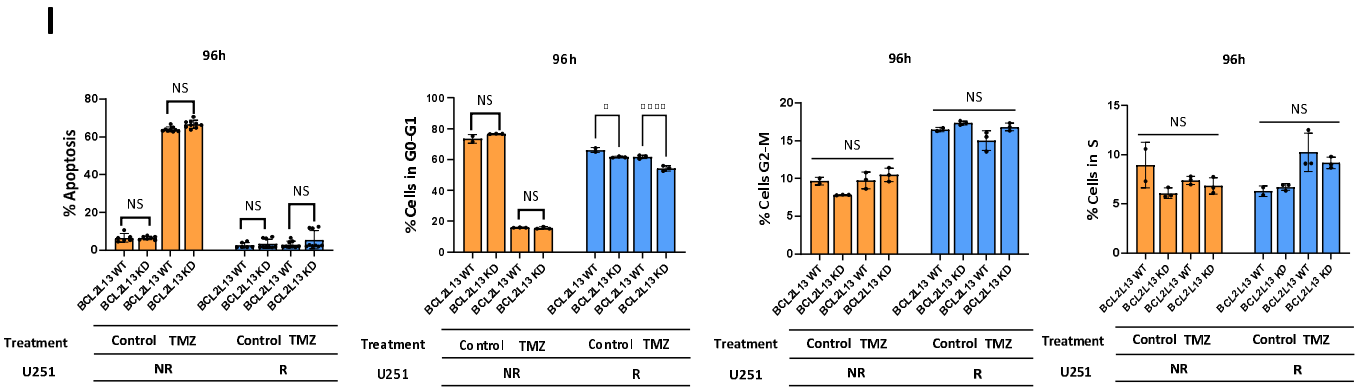

Figure 3 BCL2L13 expression is elevated in U251 TMZ-R cells and does not affect TMZ-induced apoptosis. A, B Immunoblotting analysis of BCL2L13 expression in U251 TMZ-NR and TMZ-R cells at 24, 48, and 72 hours showed significantly higher BCL2L13 in TMZ-R cells at 48 and 72 hours ($P < 0.01$), with GAPDH as a loading control. Data are representative of three biological replicates. **C** Knockdown (KD) of BCL2L13 was achieved in U251 TMZ-NR and TMZ-R cells using lentiviral infection, confirmed by immunoblotting. D, E Transmission electron microscopy (TEM) images of TMZ-NR and TMZ-R cells (scramble and BCL2L13 KD) showed no significant changes in cytosolic autophagosome numbers post-KD ($P > 0.05$), quantified across 10 cells. **F, G** Immunoblot analysis of autophagy markers in TMZ-NR and TMZ-R cells (scramble and BCL2L13 KD) after 72 hours with/without Bafilomycin-A1 (5 nM) revealed that BCL2L13 KD increased LC3β-II levels in NR cells ($P < 0.01$) without altering p62 degradation, and decreased LC3β-II levels with increased p62 degradation in R cells ($P < 0.01$). Bafilomycin-A1 significantly inhibited autophagy flux in TMZ-NR cells ($P < 0.01$) but not in TMZ-R cells. **H, I** Propidium iodide apoptosis assay and cell cycle analysis in TMZ-NR and TMZ-R cells (scramble and BCL2L13 KD) treated with TMZ (100 µM) showed no significant impact of BCL2L13 on TMZ-induced apoptosis or cell cycle distribution in either cell type at 48 and 96 hours ($P > 0.05$). Data represent three biological replicates ± SD.

BCL2L13 expression does not change mitochondrial metabolism in TMZ-resistant cells.

Previous studies have established the involvement of BCL2 family proteins in various aspects of mitochondrial function [27]. To assess the role of BCL2L13 in mitochondrial respiration, we evaluated key parameters in U251 TMZ-resistant (TMZ-R) and non-resistant (TMZ-NR) glioblastoma (GB) cells. Our findings showed that BCL2L13 expression did not significantly affect baseline respiration, maximal respiration, ATP production, proton leak, or non-mitochondrial respiration in either TMZ-NR or TMZ-R cells. However, a significant reduction in mitochondrial spare capacity was observed in TMZ-NR cells ($P < 0.0001$), while no significant change was detected in TMZ-R cells (Fig. 4B-G).

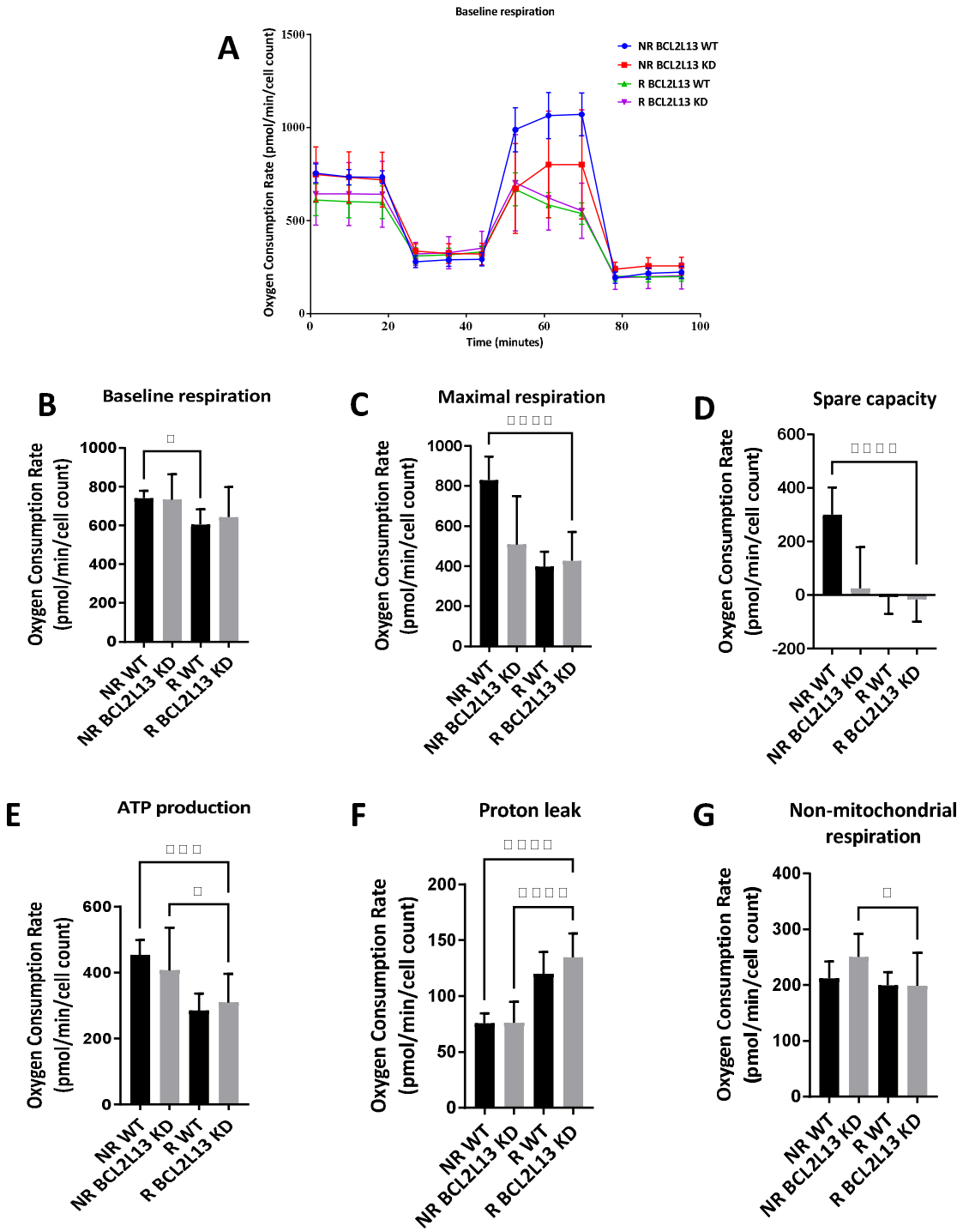
A
Baseline respiration
Oxygen Consumption Rate (pmol/min/cell count)
Time (minutes)
NR BCL2L13 WT
NR BCL2L13 KD
R BCL2L13 WT
R BCL2L13 KD
B
Baseline respiration
C
Maximal respiration
D
Spare capacity
E
ATP production
F
Proton leak
G
Non-mitochondrial respiration
NR WT
NR BCL2L13 KD
R WT
R BCL2L13 KD

Figure 4 BCL2L13 expression does not change mitochondrial metabolism in U251 TMZ-R GB cells while changing mitochondrial spare capacity in U251 TMZ-NR GB cells. **A** U251 TMZ-R and NR (BCL2L13 KD and scramble) GB cells were grown on XFe 24-well plates followed by sequential injections with different mitochondrial inhibitors (oligomycin (1μM), carbonyl cyanide-p-trifluoromethoxy-phenylhydrazone (FCCP) (1 μM), rotenone (0.5 μM) and antimycin A (0.5 μM)) to test cellular response to mitochondrial stress. Pooled data of cellular respiration in TMZ-NR and R (BCL2L13 KD and scramble) GB cells from Seahorse assays are shown. **B-G** Bar graphs demonstrate that baseline respiration, maximal respiration, spare capacity, ATP production, proton leak, and non-mitochondrial respiration are not significantly changed in TMZ-R BCL2L13-KD compared to scramble cells. Data represents the average values from triplicates of three biologically independent experiments.

A different interaction between BCL2L13 and Ceramide Synthase 2 and 6 is observed in U251 TMZ-NR and TMZ-R GB cells.

We employed co-immunoprecipitation to investigate the interactions between BCL2L13 and Ceramide Synthases 2 and 6 (CerS2 and CerS6) in U251 TMZ-resistant (TMZ-R) and non-resistant (TMZ-NR) glioblastoma (GB) cells. The results revealed that CerS6 exhibited a stronger interaction with BCL2L13 in TMZ-NR cells compared to TMZ-R cells. Conversely, CerS2 showed a weaker interaction with BCL2L13 in TMZ-NR cells compared to TMZ-R cells (Fig. 5A, B).

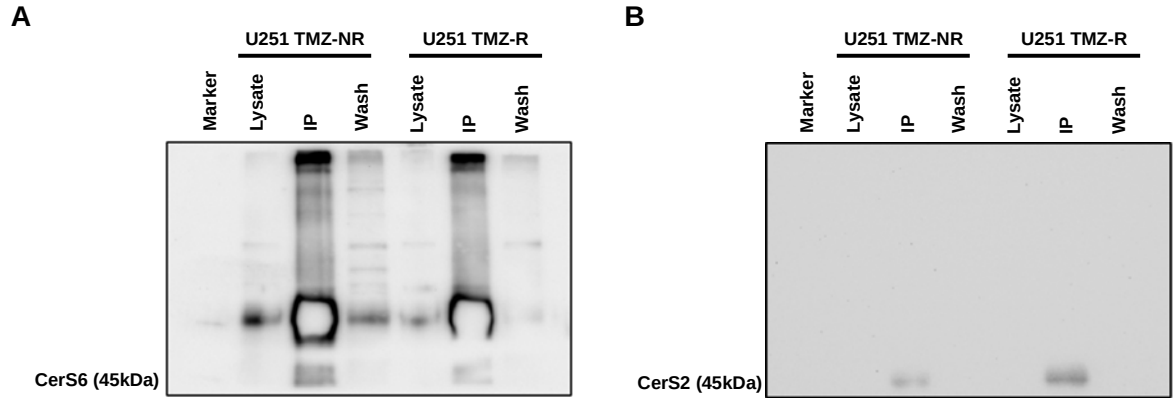

Fig. 5 BCL2L13 interacts differently with Ceramide Synthase 2 and 6 in U251 TMZ-NR and TMZ-R GBM cells. A U251 TMZ-NR and U251 TMZ-R cells were cultured for 72 hours, and cell lysates were collected for co-immunoprecipitation to determine CerS6 and BCL2L13 interaction. The results showed that CerS6 interacted more with BCL2L13 in U251 TMZ-NR cells than in U251 TMZ-R cells. **B** U251 TMZ-NR and U251 TMZ-R cells were cultured for 72 hours, and cell lysates were collected for co-immunoprecipitation to determine CerS2 and BCL2L13 interaction. Our results showed that CerS2 had lower interaction with BCL2L13 in U251 TMZ-NR cells than in U251 TMZ-R cells.

Lipidomic Profiling of U251 TMZ-Resistant and Non-Resistant GB Cells Following BCL2L13 Knockdown

Lipidomic analysis revealed significant differences between U251 TMZ-resistant (TMZ-R) and non-resistant (TMZ-NR) glioblastoma (GB) cells upon BCL2L13 knockdown. In wild-type

cells, both dhCer and MHC levels were upregulated in TMZ-R and TMZ-NR cells compared to BCL2L13 KD lines (Fig. 6A). Knockdown of BCL2L13 led to increased DHC and THC (18:0, 20:0, 22:0) in TMZ-R cells, while THC (16:0, 24:0, 24:1) levels decreased (Fig. 6A). Principal component analysis highlighted distinct lipid signatures between TMZ-R and TMZ-NR cell lines (Fig. 6B). In terms of ceramide profiles, Cer 16:0, 18:0, 20:0, 22:0, 24:0, and 24:1 were differentially expressed, with the highest levels in TMZ-R BCL2L13 KD cells (Fig. 6C). DhCer 16:0 was significantly reduced in TMZ-R BCL2L13 KD cells compared to wild-type, whereas dhCer 22:0 was elevated in TMZ-R wild-type cells (Fig. 6D). MHC and DHC levels also varied, with notable differences in their expression in both TMZ-R and TMZ-NR cells following BCL2L13 KD (Figs. 6E, 6F). THC levels exhibited similar trends, with significant alterations in the expression of specific ceramides, particularly following BCL2L13 knockdown in TMZ-R cells (Fig. 6G).

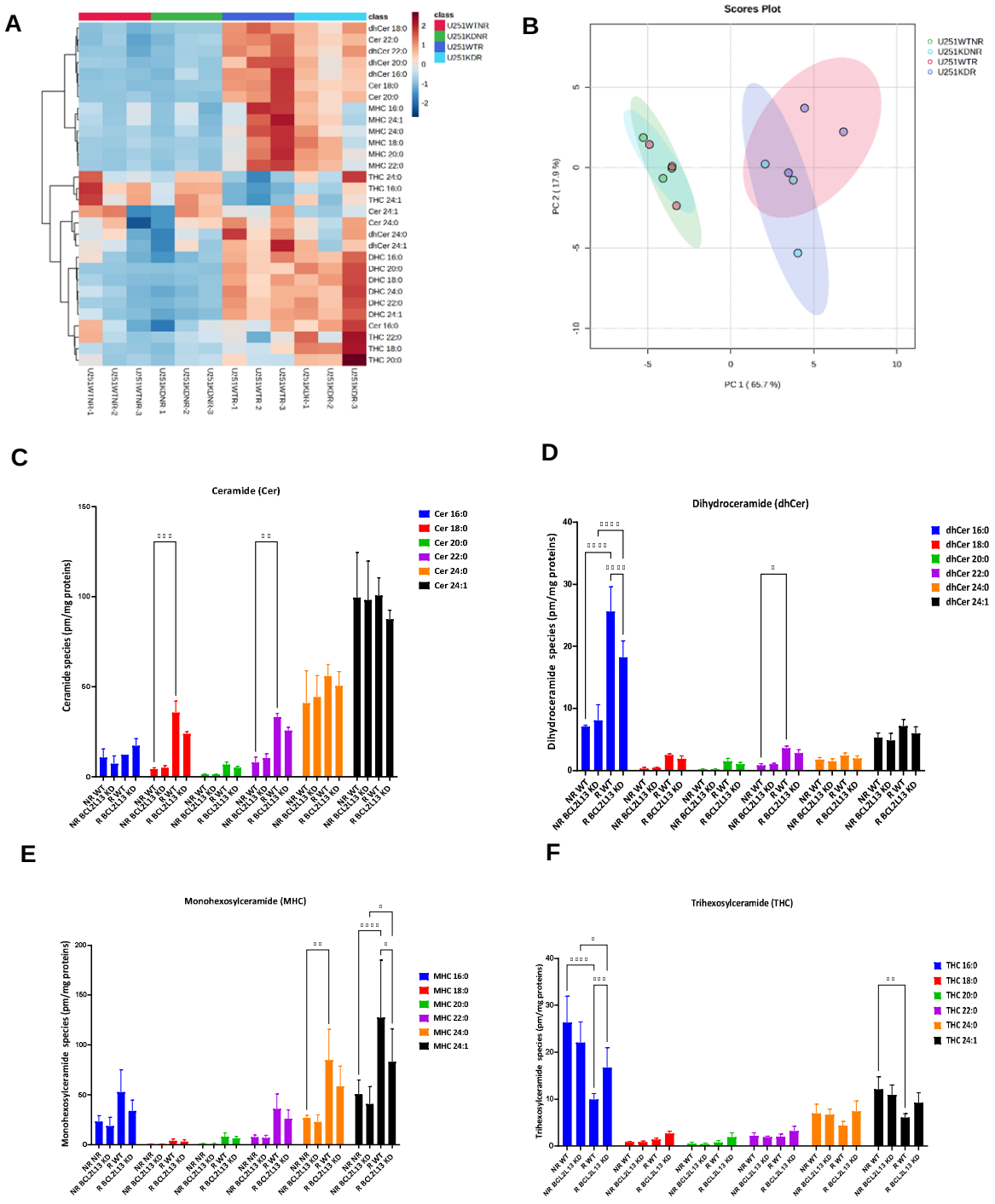
A
class
U251WTNR
U251KDNR
U251WTR
U251KDR
dhCer 18:0
Cer 22:0
dhCer 22:0
dhCer 20:0
dhCer 16:0
Cer 18:0
Cer 20:0
MHC 16:0
MHC 24:1
MHC 24:0
MHC 18:0
MHC 20:0
MHC 22:0
THC 24:0
THC 16:0
THC 24:1
Cer 24:1
Cer 24:0
dhCer 24:0
dhCer 24:1
DHC 16:0
DHC 20:0
DHC 18:0
DHC 24:0
DHC 22:0
DHC 24:1
Cer 16:0
THC 22:0
THC 18:0
THC 20:0
B
Scores Plot
PC 2 (17.9 %)
PC 1 (65.7 %)
C
Ceramide (Cer)
Ceramide species (pm/mg proteins)
Cer 16:0
Cer 18:0
Cer 20:0
Cer 22:0
Cer 24:0
Cer 24:1
D
Dihydroceramide (dhCer)
Dihydroceramide species (pm/mg proteins)
dhCer 16:0
dhCer 18:0
dhCer 20:0
dhCer 22:0
dhCer 24:0
dhCer 24:1
E
Monohexosylceramide (MHC)
Monohexosylceramide species (pm/mg proteins)
MHC 16:0
MHC 18:0
MHC 20:0
MHC 22:0
MHC 24:0
MHC 24:1
F
Trihexosylceramide (THC)
Trihexosylceramide species (pm/mg proteins)
THC 16:0
THC 18:0
THC 20:0
THC 22:0
THC 24:0
THC 24:1

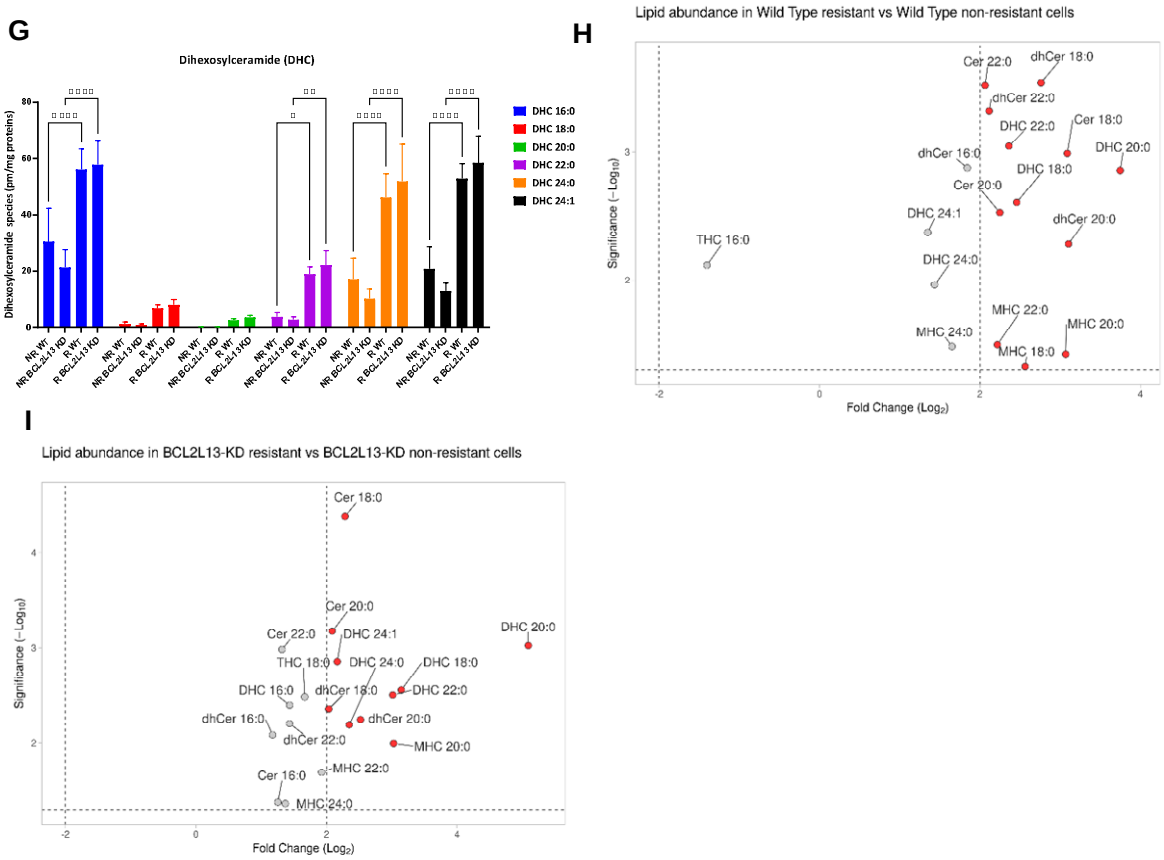

Figure 6 The effect of BCL2L13 expression on Ceramide synthase 2 and 6 downstream lipid products in TMZ-NR and TMZ-R GB cells. **A** Heatmap of ceramide family lipids across NR & R BCL2L13 WT & KD. **B** Principal Component Analysis of ceramide family lipids in NR & R BCL2L13 WT & KD groups. **C** Bar graph showing ceramide levels in non-resistant and resistant cells, with a significant increase in ceramide 18:0 ($P < 0.001$) and 22:0 ($P < 0.01$) in WT-R compared to WT-NR cells. **D** Bar graph of dihydroceramide levels in non-resistant and resistant cells, indicating a significant decrease in dihydroceramide 16:0 in BCL2L13 KD-R cells compared to WT-R ($P < 0.0001$) and BCL2L13 KD-R compared to KD-NR ($P < 0.0001$). Additionally, WT-R cells showed an increase in dihydroceramide 16:0 ($P < 0.0001$) and 22:0 ($P < 0.05$) compared to WT-NR. **E** Bar graph of monohexosylceramide levels, with a significant increase in monohexosylceramide 24:0 ($P < 0.01$) and 24:1 ($P < 0.0001$) in WT-R vs. WT-NR. Differences were also observed in BCL2L13 KD-R cells, with an increase in monohexosylceramide 24:1 compared to KD-NR ($P < 0.05$) and a decrease compared to WT-R ($P < 0.05$). **F** Bar graph of dihexosylceramide, showing significant increases in dihexosylceramide 16:0, 22:0, 24:0, and 24:1 levels in both WT-R and BCL2L13 KD-R compared to WT-NR and KD-NR (all $P < 0.0001$ for 16:0 and 24:0 in KD-R vs. KD-NR). **G** Bar graph of tetrahexosylceramide (THC) in non-resistant and resistant cells, showing significant increases in THC 16:0 in BCL2L13 KD-R vs. WT-R ($P < 0.001$) and decreases in THC 16:0 in KD-R compared to KD-NR ($P < 0.05$) and WT-R vs. WT-NR ($P < 0.0001$). THC 24:1 also showed a significant increase in WT-R compared to WT-NR ($P < 0.01$). **H, I** Lipid abundance comparisons in WT-R vs. WT-NR and BCL2L13 KD-R vs. KD-NR, with significant

lipids (red dots) indicated by a threshold fold change of 2.0 and a p-value ≤ 0.05 (shown as log scale > 1.3).

DISCUSSION

Autophagy plays a significant role in drug resistance in glioblastoma (GB), with studies indicating that autophagy can be a protective mechanism in response to treatments like temozolomide (TMZ) [28, 29]. Our study revealed that autophagy flux is notably inhibited in TMZ-resistant (R) GB cells. This finding contrasts with previous reports suggesting that elevated autophagy protein levels in high-grade gliomas result from increased autophagy turnover [30]. In our investigation, LC3βII and SQSTM1 accumulated in R cells, suggesting a blockage in the autophagy degradation process, as confirmed by bafilomycin A1 treatment. This accumulation was absent in non-resistant (NR) cells, where these proteins were effectively degraded, indicating that the elevated levels of autophagy markers in R cells are likely due to defective autophagy rather than increased autophagy activity. The data suggest that autophagy dysfunction could be a potential contributor to the resistance observed in GB cells, and targeting these pathways may enhance the efficacy of TMZ in overcoming this resistance.

BCL2L13 emerged as a potential regulator of autophagy flux, exhibiting differential effects depending on the resistance status of the GB cells. In NR cells, knocking down BCL2L13 led to increased LC3β-II levels, signifying enhanced autophagy flux. In contrast, in R cells, it decreased, suggesting that BCL2L13 may support autophagy flux in resistant cells. The impact of BCL2L13 on SQSTM1 degradation was also dependent on the resistance status; it had little effect in NR cells but significantly reduced SQSTM1 degradation in R cells. These results imply that BCL2L13 plays a crucial role in maintaining autophagy and cell survival, particularly in the context of TMZ resistance [31, 32]. This is consistent with studies showing that BCL2L13 can inhibit apoptosis by preventing mitochondrial outer membrane permeabilization (MOMP) and altering lipid synthesis, specifically through its interactions with Ceramide Synthases 2 and 6 (CerS2 and CerS6) [10, 32, 33].

The inhibition of autophagy flux is closely linked to cell cycle regulation. Disruption in autophagy can accumulate damaged cellular components, elevating oxidative stress and activating p53, which can arrest the cell cycle at the G1 phase or trigger apoptosis if the damage is beyond repair [33, 34]. The disruption of autophagy flux also interferes with the cell's energy and nutrient supply, particularly affecting the S and G2/M phases of the cell cycle, where energy demands are high [35]. This suggests that BCL2L13's autophagy regulation is crucial for cell survival and cell cycle progression in GB cells.

Our findings also demonstrated that BCL2L13 knockdown has significant effects on mitochondrial function. NR cells exhibited a considerable reduction in mitochondrial spare respiratory capacity, suggesting an impaired ability to meet energy demands. In R cells, BCL2L13 knockdown resulted in decreased ATP production and increased proton leakage, indicating mitochondrial dysfunction. This highlights BCL2L13's role in maintaining mitochondrial integrity and function, particularly in TMZ-resistant cells, where mitochondrial health is critical for survival [10, 36, 37]. BCL2L13's involvement in mitochondrial metabolism, particularly in balancing glycolysis and oxidative phosphorylation, underscores its importance in GB cell survival under stress conditions [38, 39].

A key aspect of our study was the lipidomic analysis, which revealed distinct ceramide profiles between TMZ-NR and TMZ-R cells. BCL2L13 interacts with CerS2 and CerS6, inhibiting their activity, with the strength of these interactions influencing the levels of various ceramides [10]. In TMZ-NR cells, BCL2L13 strongly interacts with CerS6, which should lead to significant inhibition of its activity compared to TMZ-R cells based on its effect on enzyme activity. Conversely, CerS2 interaction with BCL2L13 is weaker in NR cells, resulting in less inhibition and higher ceramide levels in R cells. This differential regulation is evident in the distinct ceramide profiles observed, where dihydroceramide (dhCer) and monohexosylceramide (MHC) levels were elevated in wild-type cells compared to BCL2L13

knockdown lines. Additionally, suppressing BCL2L13 led to increased levels of dihexosylceramide (DHC) and trihexosylceramide (THC) in R cells, suggesting a critical role for BCL2L13 in modulating ceramide synthesis and influencing GB cell survival [40-43].

The differential ceramide profiles observed in TMZ-resistant (TMZ-R) and non-resistant (TMZ-NR) GB cells are potentially linked to autophagy flux and BCL2L13 expression. In TMZ-NR cells, active autophagy flux correlates with lower levels of specific ceramides, such as Cer 16:0 and 24:1, compared to TMZ-R cells, indicating that autophagy may facilitate the degradation or utilization of these lipids [44]. In contrast, TMZ-R cells exhibit inhibited autophagy flux, accumulating ceramides like Cer 18:0, 20:0, 22:0, and 24:0, associated with resistance mechanisms and cell survival [45-47]. Given that BCL2L13 inhibits CerS activity, its knockdown would be expected to increase ceramide synthesis. However, our results showed that BCL2L13 knockdown did not fully restore autophagy flux or significantly alter ceramide levels in a way that sensitizes TMZ-R cells to apoptosis. This suggests that while BCL2L13 modulates ceramide metabolism, additional pathways might be compensating to maintain resistance. Therefore, targeting CerS2 and CerS6 more directly, combined with autophagy modulation, could provide a more effective strategy to overcome chemoresistance in GB cells.

Given the findings of this study, future research should focus on targeting ceramide metabolism as a potential therapeutic strategy for overcoming TMZ resistance in GB. The differential regulation of CerS2 and CerS6 by BCL2L13 in resistant versus non-resistant cells suggests that modulating ceramide synthesis could restore sensitivity to TMZ in resistant GB cells. Specifically, strategies that either enhance CerS6 activity or inhibit CerS2 could be explored to disrupt the survival mechanisms of TMZ-resistant GB cells. Additionally, further investigation into the role of BCL2L13 in mitochondrial function and its broader implications in GB pathophysiology could provide new insights into targeting mitochondrial pathways in GB therapy.

DATA AVAILABILITY: Data will be available by corresponding author.

ACKNOWLEDGEMENTS: The authors acknowledge CHATGPT 4o for professional English edit.

AUTHOR CONTRIBUTIONS: Courtney Clark (C.C.) conducted all experimental work and prepared the methods section. Amir Barzegar-Behrooz (A.B.B.) drafted the manuscript and performed the literature review. Simone C. da Silva Rosa (S.C.S.R.), Jaodi Jacobs (J.J.), and Xiaohui Wang (X.W.) conducted the lipidomics analysis and prepared the related figures. Abhay Srivastava (A.S.) performed the Seahorse assays and analyzed the data. Rui Vitorino (R.V.) supervised the lipidomics analysis and contributed to drafting the lipidomics section. Sudharsan Rao Ande (S.R.A.) established and executed the Co-immunoprecipitation (Co-IP) experiments. Amir Ravandi (A.R.) led the lipidomics experimental planning. Sanjiv Dhingra (S.D.) provided supervision and leadership in mitochondrial metabolism analysis. Stevan Pecic (S.P.) contributed to supervision, resources, and initial manuscript drafting. Donal Miller (D.M.) provided supervision, resources, and conceptualization of the study. Shahla Shojaei (S.S.) developed the TMZ-resistant cells, contributed to project design and conceptualization. Saeid Ghavami (S.G.) led and supervised the project, oversaw study design, and secured resources.

FUNDING. Research reported in this publication was partially supported by the National Institute of General Medical Sciences of the National Institutes of Health (NIH) under award number 1 R16GM149204-02 to SP. The content is solely the responsibility of the authors and does not necessarily represent the official views of the National Institutes of Health (NIH). SG

and DM was supported by UCRP operating grant. SCSR was supported by CIHR PDF fellowship. AR was supported by Heart and Stroke Foundation grant.

COMPETING INTERESTS. Authors did not have any competing interest.

ADDITIONAL INFORMATION: N/A

REFERENCES

1. Barzegar Behrooz, A., et al., *Genetic Prognostic Factors in Adult Diffuse Gliomas: A 10-Year Experience at a Single Institution.* Cancers, 2024. **16**(11): p. 2121.
2. Molinaro, A.M., et al., *Genetic and molecular epidemiology of adult diffuse glioma.* Nature Reviews Neurology, 2019. **15**(7): p. 405-417.
3. Wu, W., et al., *Glioblastoma multiforme (GBM): An overview of current therapies and mechanisms of resistance.* Pharmacological Research, 2021. **171**: p. 105780.
4. Wan, S., et al., *Pyroptosis, ferroptosis, and autophagy cross-talk in glioblastoma opens up new avenues for glioblastoma treatment.* Cell Commun Signal, 2023. **21**(1): p. 115.
5. Kao, T.J., et al., *Dysregulated lipid metabolism in TMZ-resistant glioblastoma: pathways, proteins, metabolites and therapeutic opportunities.* Lipids Health Dis, 2023. **22**(1): p. 114.
6. Liu, J., et al., *Selective autophagy in cancer: mechanisms, therapeutic implications, and future perspectives.* Mol Cancer, 2024. **23**(1): p. 22.
7. Behrooz, A.B., et al., *The obesity-autophagy-cancer axis: Mechanistic insights and therapeutic perspectives.* Semin Cancer Biol, 2024. **99**: p. 24-44.
8. Clark, C., et al., *Assessing Autophagy Flux in Glioblastoma Temozolomide Resistant Cells.* bioRxiv, 2024: p. 2024.08.09.607348.
9. Jacobs, J., et al., *The role of BCL2L13 in glioblastoma: turning a need into a target.* Biochem Cell Biol, 2024. **102**(2): p. 127-134.
10. Jensen, S.A., et al., *Bcl2L13 is a ceramide synthase inhibitor in glioblastoma.* Proc Natl Acad Sci U S A, 2014. **111**(15): p. 5682-7.
11. Meng, F., et al., *Down-regulation of BCL2L13 renders poor prognosis in clear cell and papillary renal cell carcinoma.* Cancer Cell Int, 2021. **21**(1): p. 332.
12. Wajapeyee, N., T.C. Beamon, and R. Gupta, *Roles and therapeutic targeting of ceramide metabolism in cancer.* Mol Metab, 2024. **83**: p. 101936.
13. Tugrul, F., C. Vejselova Sezer, and H.M. Kutlu, *Proapoptotic effects of ceranib-2 in combination with radiation therapy on human breast cancer cells.* Eur Rev Med Pharmacol Sci, 2024. **28**(6): p. 2322-2328.
14. McDermott, M., et al., *In vitro Development of Chemotherapy and Targeted Therapy Drug-Resistant Cancer Cell Lines: A Practical Guide with Case Studies.* Front Oncol, 2014. **4**: p. 40.
15. Ghavami, S., et al., *Geranylgeranyl transferase 1 modulates autophagy and apoptosis in human airway smooth muscle.* Am J Physiol Lung Cell Mol Physiol, 2012. **302**(4): p. L420-8.
16. Ghavami, S., et al., *Airway mesenchymal cell death by mevalonate cascade inhibition: integration of autophagy, unfolded protein response and apoptosis focusing on Bcl2 family proteins.* Biochim Biophys Acta, 2014. **1843**(7): p. 1259-71.
17. Alizadeh, J., et al., *Evaluation of Mitochondrial Phagy (Mitophagy) in Human Non-small Adenocarcinoma Tumor Cells.* Methods Mol Biol, 2024.
18. Alizadeh, J., et al., *Inhibition of Autophagy Flux Promotes Secretion of Chondroitin Sulfate Proteoglycans in Primary Rat Astrocytes.* Mol Neurobiol, 2021. **58**(12): p. 6077-6091.
19. Kawalec, P., et al., *Differential impact of doxorubicin dose on cell death and autophagy pathways during acute cardiotoxicity.* Toxicol Appl Pharmacol, 2022. **453**: p. 116210.
20. Brun, P., et al., *The regulatory activity of autophagy in conjunctival fibroblasts and its possible role in vernal keratoconjunctivitis.* J Allergy Clin Immunol, 2020. **146**(5): p. 1210-1213 e9.
21. Dastghaib, S., et al., *Simvastatin Induces Unfolded Protein Response and Enhances Temozolomide-Induced Cell Death in Glioblastoma Cells.* Cells, 2020. **9**(11).

22. Dastghaib, S., et al., *Correction: Dastghaib et al. Simvastatin Induces Unfolded Protein Response and Enhances Temozolomide-Induced Cell Death in Glioblastoma Cells. Cells 2020, 9, 2339.* Cells, 2024. **13**(8).
23. Alizadeh, J., et al., *Autophagy modulates transforming growth factor beta 1 induced epithelial to mesenchymal transition in non-small cell lung cancer cells.* Biochim Biophys Acta Mol Cell Res, 2018. **1865**(5): p. 749-768.
24. Alizadeh, J., et al., *Mevalonate Cascade Inhibition by Simvastatin Induces the Intrinsic Apoptosis Pathway via Depletion of Isoprenoids in Tumor Cells.* Sci Rep, 2017. **7**: p. 44841.
25. Hajiahmadi, S., et al., *Temozolomide, Simvastatin and Acetylshikonin Combination Induces Mitochondrial-Dependent Apoptosis in GBM Cells, Which Is Regulated by Autophagy.* Biology (Basel), 2023. **12**(2).
26. Surendran, A., et al., *Impact of myocardial reperfusion on human plasma lipidome.* iScience, 2022. **25**(2): p. 103828.
27. Kale, J., E.J. Osterlund, and D.W. Andrews, *BCL-2 family proteins: changing partners in the dance towards death.* Cell Death Differ, 2018. **25**(1): p. 65-80.
28. Sanati, M., et al., *Recent advances in glioblastoma multiforme therapy: A focus on autophagy regulation.* Biomed Pharmacother, 2022. **155**: p. 113740.
29. Khan, I., et al., *Deciphering the Role of Autophagy in Treatment of Resistance Mechanisms in Glioblastoma.* Int J Mol Sci, 2021. **22**(3).
30. Barciszewska, A.M., et al., *A New Epigenetic Mechanism of Temozolomide Action in Glioma Cells.* PLoS One, 2015. **10**(8): p. e0136669.
31. Bilger, A., et al., *FET-PET-based reirradiation and chloroquine in patients with recurrent glioblastoma: first tolerability and feasibility results.* Strahlenther Onkol, 2014. **190**(10): p. 957-61.
32. Zheng, K., et al., *Selective Autophagy Regulates Cell Cycle in Cancer Therapy.* Theranostics, 2019. **9**(1): p. 104-125.
33. Mathiassen, S.G., D. De Zio, and F. Cecconi, *Autophagy and the Cell Cycle: A Complex Landscape.* Front Oncol, 2017. **7**: p. 51.
34. Ziegler, D.V., K. Huber, and L. Fajas, *The Intricate Interplay between Cell Cycle Regulators and Autophagy in Cancer.* Cancers (Basel), 2021. **14**(1).
35. Mizushima, N. and D.J. Klionsky, *Protein turnover via autophagy: implications for metabolism.* Annu Rev Nutr, 2007. **27**: p. 19-40.
36. Song, C., et al., *Mitophagy: A novel perspective for insighting into cancer and cancer treatment.* Cell Prolif, 2022. **55**(12): p. e13327.
37. Wang, J., et al., *BCL2L13 promotes mitophagy through DNM1L-mediated mitochondrial fission in glioblastoma.* Cell Death Dis, 2023. **14**(9): p. 585.
38. Meng, F., et al., *BCL2L13: physiological and pathological meanings.* Cell Mol Life Sci, 2021. **78**(6): p. 2419-2428.
39. Chen, W., H. Zhao, and Y. Li, *Mitochondrial dynamics in health and disease: mechanisms and potential targets.* Signal Transduction and Targeted Therapy, 2023. **8**(1): p. 333.
40. Lachkar, F., et al., *Dihydroceramides: their emerging physiological roles and functions in cancer and metabolic diseases.* Am J Physiol Endocrinol Metab, 2021. **320**(1): p. E122-e130.
41. Zheng, W., et al., *Ceramides and other bioactive sphingolipid backbones in health and disease: lipidomic analysis, metabolism and roles in membrane structure, dynamics, signaling and autophagy.* Biochim Biophys Acta, 2006. **1758**(12): p. 1864-84.
42. Gagliostro, V., et al., *Dihydroceramide delays cell cycle G1/S transition via activation of ER stress and induction of autophagy.* Int J Biochem Cell Biol, 2012. **44**(12): p. 2135-43.
43. Noack, J., et al., *A sphingosine kinase inhibitor combined with temozolomide induces glioblastoma cell death through accumulation of dihydrosphingosine and dihydroceramide, endoplasmic reticulum stress and autophagy.* Cell Death Dis, 2014. **5**(9): p. e1425.
44. Lin, Z., et al., *The lipid basis of cell death and autophagy.* Autophagy, 2024. **20**(3): p. 469-488.

45. Hartmann, D., et al., *The equilibrium between long and very long chain ceramides is important for the fate of the cell and can be influenced by co-expression of CerS.* The International Journal of Biochemistry & Cell Biology, 2013. **45**(7): p. 1195-1203.
46. Bassi, R., et al., *Ceramide Is Involved in Temozolomide Resistance in Human Glioblastoma U87MG Overexpressing EGFR.* Int J Mol Sci, 2023. **24**(20).
47. Wajapeyee, N., T.C. Beamon, and R. Gupta, *Roles and therapeutic targeting of ceramide metabolism in cancer.* Molecular Metabolism, 2024. **83**: p. 101936.